Available online at www.sciencedirect.com

ScienceDirect

Acta Materialia 93 (2015) 87–94

Acta MATERIALIA

www.elsevier.com/locate/actamat

Irradiation-induced formation of a spinel phase at the FeCr/MgO interface

Yun Xu,[a,b,1] Satyesh Kumar Yadav,[a,1] Jeffery A. Aguiar,[a] Osman Anderoglu,[a] Jon Kevin Baldwin,[c] Yongqiang Wang,[a] Amit Misra,[d] Hongmei Luo,[b] Blas P. Uberuaga[a] and Nan Li[c,*]

[a] *Materials Science and Technology Division, MST-8, Los Alamos National Laboratory, Los Alamos, NM 87545, USA*
[b] *Department of Chemical and Materials Engineering, New Mexico State University, Las Cruces, NM 88003, USA*
[c] *Materials Physics and Applications Division, MPA-CINT, Los Alamos National Laboratory, Los Alamos, NM 87545, USA*
[d] *Department of Materials Science and Engineering, University of Michigan, Ann Arbor, MI 48109, USA*

Received 20 January 2015; revised 9 March 2015; accepted 26 March 2015
Available online 27 April 2015

Abstract—Oxide dispersion strengthened ferritic/martensitic alloys have attracted significant attention for their potential uses in future nuclear reactors and storage vessels, as the metal/oxide interfaces act as stable high-strength sinks for point defects while also dispersing helium. Here, in order to unravel the evolution and interplay of interface structure and chemistry upon irradiation in these types of materials, an atomically sharp FeCr/MgO interface was synthesized at 500 °C and separately annealed and irradiated with Ni^{3+} ions at 500 °C. After annealing, a slight enrichment of Cr atoms was observed at the interface, but no other structural changes were found. However, under irradiation, sufficient Cr diffuses across the interface into the MgO to form a Cr-enriched transition layer that contains spinel precipitates. First-principles calculations indicate that it is energetically favorable to incorporate Cr, but not Fe, substitutionally into MgO. Our results indicate that irradiation can be used to form new phases and complexions at interfaces, which may have different radiation tolerance than the pristine structures.
Published by Elsevier Ltd. on behalf of Acta Materialia Inc.

Keywords: Metal/oxide interfaces; Spinel phase; DFT calculations

1. Introduction

Metal/oxide interfaces have played a critical role in a variety of industrial fields with significant ramifications for structural composites, electroceramic devices, and environmental coatings especially with nuclear-energy applications [1–6]. The unique properties of such interfaces rely on the transition from the delocalized metallic bonding to ionic or covalent bonding in oxides. How the crystallography of metals orients with oxides and especially how the first metal layer bonds with the adjoining oxide layer at the interface will, to a large extent, determine the properties of the whole composite, and thus have become the focus of extensive study [1–6].

Because of commercial viability, high purity single-crystal MgO has been widely used as a model substrate to synthesize epitaxial metal films and to investigate the atomic configuration of heterointerfaces. Generally, when face centered cubic (fcc) metals are epitaxially grown on MgO (100), the preferred orientation relationship is (100) metal ‖ (100) MgO & [001] metal ‖ [001] MgO (referred to here as OR-I) [7,8]. The orientation relationship changes to (111) metal ‖ (111) MgO & [110] metal ‖ [110] MgO (OR-II) when metals are synthesized on MgO (111) substrates [9,10]. In both cases, fcc metals prefer to bind on top of oxygen. These features seem to be independent of the lattice mismatch between metals and MgO, since the general relationship applies equally well for a variety of systems, such as Ag/MgO (3%), Pd/MgO (7.6%) and even Cu/MgO (14.2%). In order to accommodate the lattice mismatch induced strain, misfit dislocations tend to dissociate into partials for these interfaces, in particular $1/2a_{metal}\langle 100\rangle$ for OR-I and $1/6a_{metal}\langle 112\rangle$ for OR-II [11,12]. Bollmann's O-lattice theory accurately predicts the interfacial misfit dislocation network [12,13]. Atomic and electronic-structure calculations have explored the structural features in detail for the Ag/MgO system: (i) for the MgO surface, the most favorable adsorption site of Ag atoms changes depending on the coverage of the metal atoms on the surface [14,15]; (ii) the distance between the first Ag plane and MgO surface is expanded with respect to both Ag and MgO (001) inter-planar distances [16].

The situation becomes more complicated when body centered cubic (bcc) metals are deposited on MgO substrates. Wang et al. uncovered the interface orientation relationship of single crystal Cr epitaxially grown on MgO – Cr (100) ‖ MgO (100) & Cr [110] ‖ MgO [100] (OR-III) – and they reported that the misfit dislocation spacing is less than the theoretical prediction [17]. Their

* Corresponding author. Tel.: +1 505 665 1857; e-mail: nanli@lanl.gov

[1] These authors contributed equally to this work.

http://dx.doi.org/10.1016/j.actamat.2015.03.042
1359-6462/Published by Elsevier Ltd. on behalf of Acta Materialia Inc.

experimental analysis revealed that Cr atoms reside on top of O atoms. First principle calculations [18] explored the preference of the bcc metals Fe, Cr and V on top of O atoms on the MgO (001) surface. However, Ikuhara et al. found that, for the interface structure of V/MgO, although the orientation relationship follows the same rule, the V atoms locate themselves directly on top of the Mg atoms [19,20]. Meanwhile, the distribution and Burgers vectors of misfit dislocations may be influenced by the interface morphology [21,22]. In the Nb/MgO system, due to interfacial faceting, the orientation relationship may change to Nb (110) ‖ MgO (100) & Nb [111] ‖ MgO [011] (OR-IV) [21].

Recently, new applications of metal/oxide interfaces focusing on the enhancement of radiation tolerance, where the interfaces act as stable high-strength sinks for point defects by assisting the recombination process between interstitials and vacancies, have been reported [23]. Containing widely distributed nanosized oxide particles, oxide dispersion strengthened (ODS) ferritic/martensitic alloys exhibit high temperature creep strength [23] over traditional stainless steel. However, under irradiation, the elemental redistribution at boundaries or the change of oxide particle size commences [24–27], where the corresponding sink strength may be altered. Studying these complex ODS materials is rather difficult because of (i) the complex chemical composition of both matrix steels and oxide particles [28]; (ii) the challenge to probe the chemical composition of embedded three dimensional oxide nanoparticles (although atom-probe tomography (APT) has been widely applied to obtain 3D reconstructions of elemental components [26,29,30], however, the extraction of quantitative chemical profiles around interfaces from APT is not straightforward); and (iii) the wide distribution of particle size [23]. Thus the use of model metal/oxide interfaces provides a route to uncover the fundamental behavior associated with the interfaces [31,32]. Here, Fe 12 at.% Cr has been epitaxially grown at 500 °C using single crystal MgO (100) as substrate. The resulting atomically sharp metal/oxide interface provides a clean reference to examine Cr solute redistribution and the ensuing structure/phase evolution under irradiation.

2. Experimental methods

The 100 nm FeCr layer was fabricated at 500 °C on MgO (100) substrate using co-sputtering in a high vacuum chamber with a base pressure of $\leqslant 5.0 \times 10^{-8}$ torr. Two sources were used simultaneously with independent shutters and power supplies. The Fe power ran at 400 watts and the Cr power at 60 watts, in order to achieve approximate atomic ratios of 6.8 Fe to 1 Cr. The deposition rate was approximately 0.4 nm/s, with the total time of the deposition being 250 s. 10 MeV Ni^{3+} ions were utilized to irradiate the film at 500 °C to a fluence of 10^{16} ions/cm^2. The elapsed time of the irradiation, performed at the Ion Beam Materials Laboratory at Los Alamos National Laboratory (LANL), was ~1 h. For comparison, a second as-synthesized sample was annealed at 500 °C for 1 h. The Monte Carlo simulation code Stopping and Range of Ions in Matter (SRIM) [33–35] was used (the displacement threshold energies used for all 4 species were 25 eV while the calculations were performed in "quick" Kinchin and Pease mode) to determine the level of displacements per atom (dpa): ~10 dpa in the metal layer and ~3 dpa in the oxide layer (in the region near the interface). Analytical aberration corrected microscopy was performed on the image-corrected FEI Titan equipped with a Gatan Tridiem electron energy loss image filter (GIF) at LANL, operating in transmission electron microscopy (TEM) mode at 300 keV. Scanning TEM (STEM) high angle annular dark field (HAADF) and electron energy-loss spectrometry (EELS) was performed using the probe-corrected FEI Titan operated at 300 and the Nion UltraSTEM at 100 keV at Oak Ridge National Laboratory.

3. Results

The microstructure of the as-deposited thin film is shown in Fig. 1. The cross-sectional TEM image (Fig. 1a) was taken in-zone. The dark lines in the FeCr film are threading misfit dislocations. The electron diffraction pattern in Fig. 1b reveals that the FeCr film grown on the MgO substrate adopted a cube-on-cube relationship with a 45° in-plane rotation: MgO (100) ‖ FeCr (200) & MgO [100] ‖ FeCr [110] (OR-III). The high resolution TEM image in Fig. 1c shows an atomically sharp interface. Observed along the FeCr [110] or MgO [100] direction, interfacial misfit dislocations can be identified as an extra atomic plane in the metal layer. All misfit dislocations reside at the interface with uneven spacing. The average spacing, measured by collecting multiple atomic resolution TEM micrographs at different locations (not all shown here), is ~4.8 nm, slightly larger than the theoretical prediction (4.2 nm). This may indicate that the interfacial strain is not fully relaxed. A magnified image of one misfit dislocation is shown in Fig. 1d. The corresponding Burgers circuit (starting at S and ending at F) has been drawn to identify the Burgers vector ($\boldsymbol{b} = \frac{1}{2}a_{FeCr}$ [110]). Energy dispersive X-ray spectroscopy (EDS) line scans were performed normal to the interface to show the compositional variation for different chemical elements (in Fig. 1e). The profile of Cr presents a little bump but no interdiffusion at the interface region.

In order to better understand the thermal behavior of the system, in contrast to the irradiation-induced behavior discussed below, the synthesized sample was annealed for one hour at 500 °C. After annealing, there is no observed structural change in either the FeCr or MgO layers. However, the EDS line scan in Fig. 2a shows obvious segregation of Cr toward the interface. For comparison, the Cr elemental EDS profiles of the synthesized and annealed samples have been overlapped and are presented in Fig. 2b. This result indicates that Cr is thermodynamically attracted to the interface, likely a consequence of the stronger interaction of Cr than Fe with oxygen.

The microstructure of the irradiated thin film is shown in Fig. 3a. Under heavy ion irradiation, a transition layer is formed on the MgO side of the FeCr/MgO interface. The dark field high resolution STEM image of the irradiated interface shown in Fig. 3b reveals that the thickness of the transition layer is ~3.3 nm, based on the stark difference in atomic contrast due to the presence of Cr. Irradiation effects on the thickness of the transition layer will be evaluated in future work, which may be related to radiation-induced diffusion or ballistic impact. The

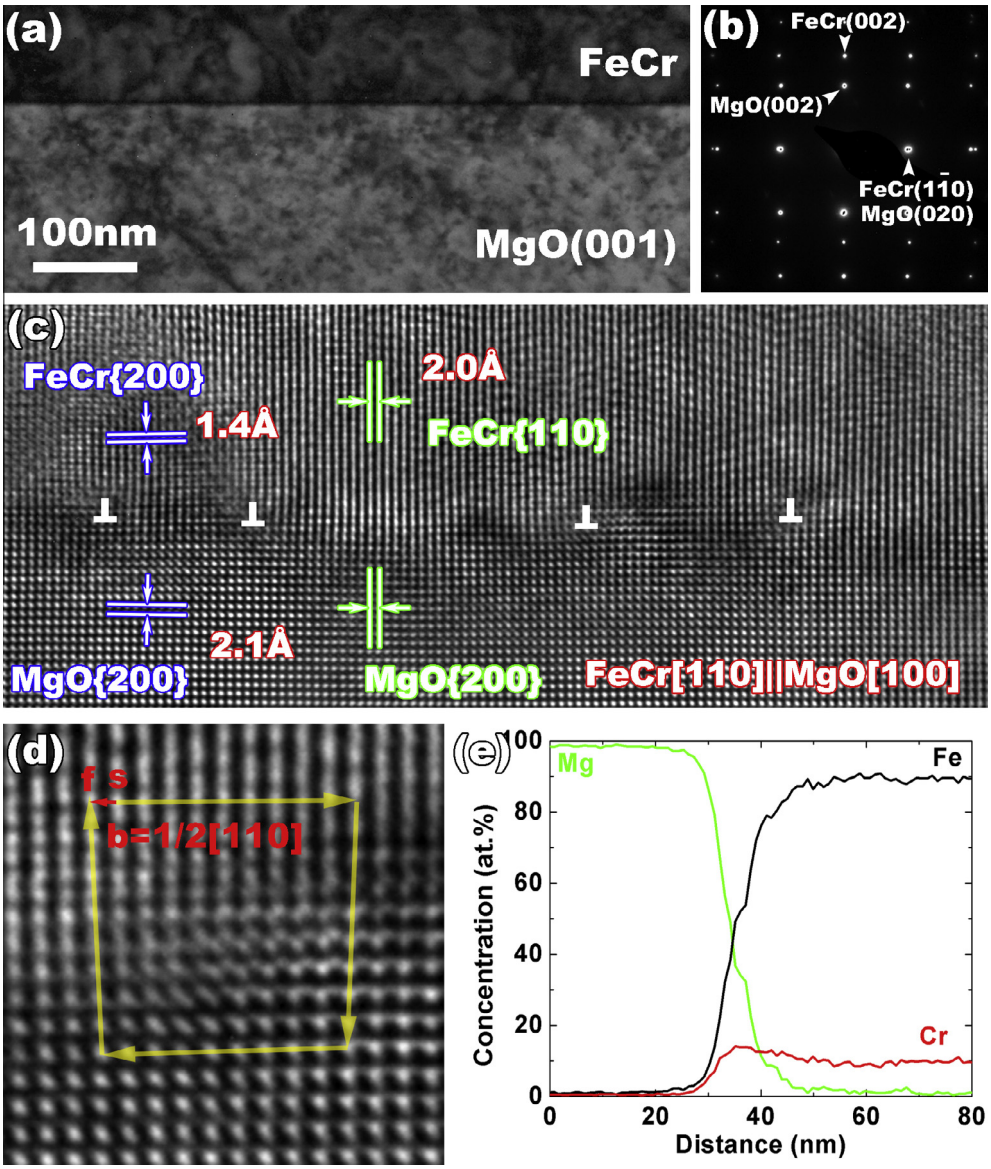

Fig. 1. Microstructure of and chemical distribution at the pristine FeCr/MgO interface. (a) Bright field cross-sectional TEM image of FeCr/MgO interface. (b) Corresponding electron diffraction pattern. (c) High resolution TEM image of the interface. (d) Magnified image of the interface, highlighting the structure of the misfit dislocation. (e) EDS profile of Fe, Mg and Cr across the as-grown interface.

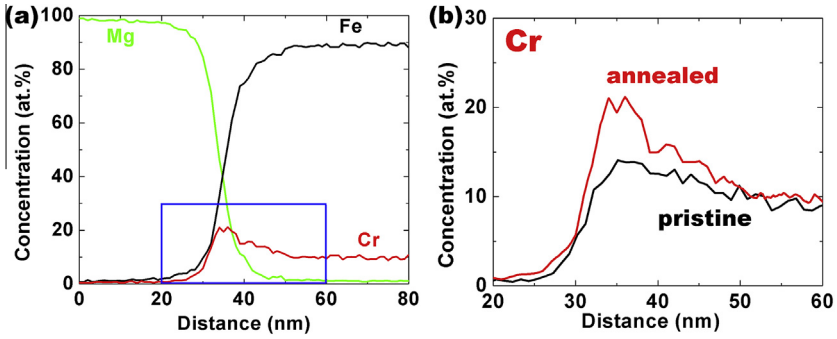

Fig. 2. Chemical analysis of the FeCr/MgO interface. (a) EDS composition profiles show the diffusion of Cr toward the interface after annealing. (b) Overlapping of the Cr profiles of pristine and annealed samples at the interface.

majority of the transition layer has the same structure as MgO. A magnified high resolution TEM micrograph presents an isolated misfit dislocation, with Burgers vector of $\frac{1}{2}a_{MgO}$ [1 0 0], at the interface between MgO and the nucleated transition layer (as shown in Fig. 3c), indicating the periodic unit in the transition layer is close to, but smaller

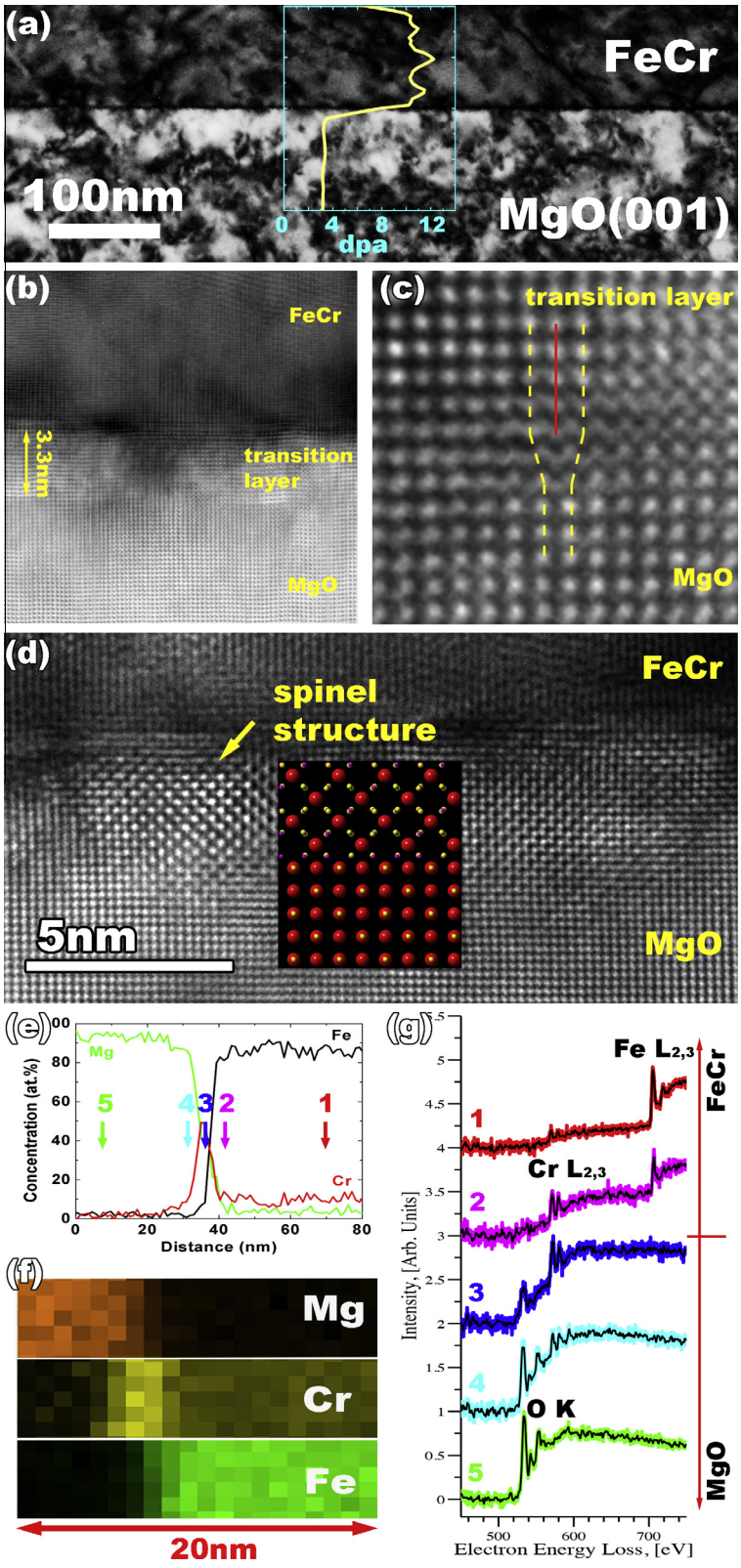

Fig. 3. Microstructure of and chemical distribution at the irradiated FeCr/MgO interface. (a) Bright field cross-sectional TEM image of the irradiated FeCr/MgO interface with SRIM profile superimposed. (b) Dark field high resolution STEM image of the irradiated interface revealing the thickness of the transition layer is ~3.3 nm. (c) High resolution TEM image to characterize the structure of the misfit dislocation between the transition layer and the MgO substrate. (d) High resolution TEM micrograph identifying the structure of the transition layer and small regions with the spinel structure, as indicated by the arrow. The inset shows an atomic model of the structure of these regions, containing both MgO and spinel. (e) EDS line and (f) two-dimensional mapping of Fe, Mg and Cr across the irradiated interface. (g) EELS line scans performed at five different locations parallel to the FeCr/MgO interface, as indicated in (e), reveal the valence state of Cr at the interface.

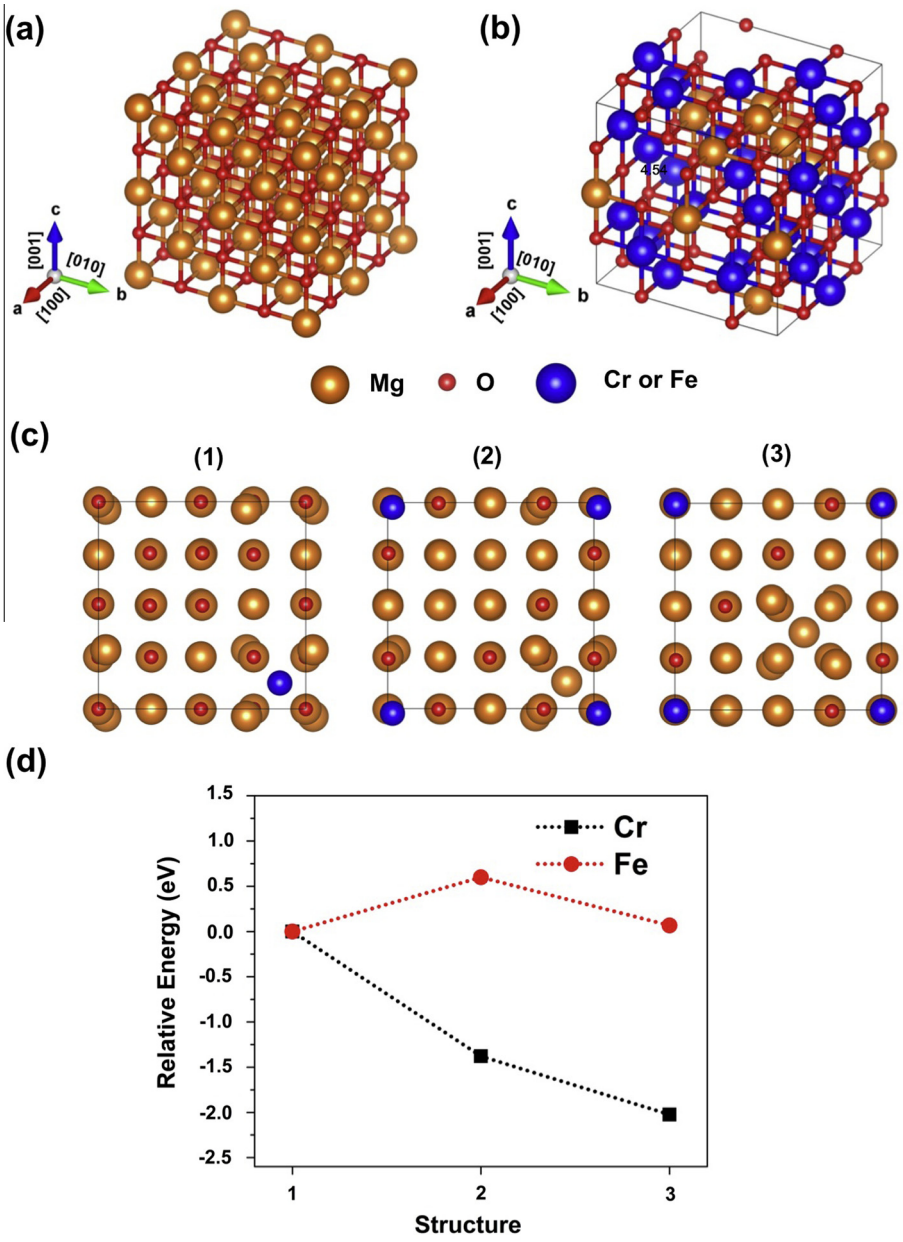

Fig. 4. (a) MgO in rocksalt crystal structure and (b) $MgCr_2O_4$ with 3 Mg replaced by 2 Cr, forming defective rocksalt structure. (c) Atomic structures of supercells containing Cr or Fe defects and (d) the relative formation energy of various structures. The structures represent: (1) Cr or Fe at an interstitial position, (2) and (3) Cr or Fe at substitutional position and Mg at an interstitial position with increasing distance from the Cr or Fe substitutional atom.

than, that in MgO. The magnified high resolution TEM image revealed that a certain region of the transition layer has the spinel structure, as indicated by the arrow and the inset of the atomic structure in Fig. 3d [36], and the corresponding thickness is ~3 nm as well. Average EDS line profiles and 2-dimensional spectral maps have been collected to quantify the chemical composition after irradiation (in Fig. 3e and f). Compared to the chemical profile of Fe, which shows no measurable intermixing across the interface, Cr diffused toward and segregated at the interface. The location of the Cr enrichment corresponds to the transition layer. Based on the integration of the peak profile, the stoichiometry ratio of Mg:Cr is close to 1:2 in the transition layer. Further, the chemical valence of Fe, Cr and O across the interface has been probed by atomically resolved EELS, as shown in Fig 3g. After irradiation, the chromium content extends beyond the interface and builds up at the interface. In contrast to the slight enrichment on the metal side observed after annealing, after irradiation the Cr is on MgO side. The ionic valence state of chromium at the interface (calculated from the intensity ratio of L_3/L_2 at position 3 in Fig. 3g) is 3 ± 0.1 electrons, consistent with the presence of Cr^{3+} at the irradiated interface, suggesting that the spinel-structured precipitates are $MgCr_2O_4$ while the remainder of the transition layer is Cr-rich disordered rocksalt with a similar stoichiometry of $MgCr_2O_4$. With the current analysis, we cannot establish any relationship between the formation of $MgCr_2O_4$ spinel and the location of misfit dislocations. *In situ* irradiation could be used to correlate the formation of spinel with the structural features of the

interface and will be performed in the future. We note that, under irradiation, spinels often transform to chemically identical and structurally related disordered rocksalt, in which the A and B cations are randomly distributed across the various cation sites in the rocksalt structure. Finally, a large number of defect clusters have been observed close to the interface in both materials, but no amorphous region has been observed either at the interface or inside MgO after irradiation, as expected from former studies [37–39].

4. Discussion

Exactly why chromium incorporates into MgO to form $MgCr_2O_4$, while iron does not is key to understanding the evolution of this particular metal/oxide interface. To provide insights into this question, density functional theory (DFT) calculations, using the Vienna Ab initio Simulation Package (VASP) [40], have been performed, in which the Perdew, Burke, and Ernzerhof (PBE) [41] generalized gradient approximation (GGA) exchange–correlation functional and the projector-augmented wave (PAW) method [42] have been employed. For all the calculations, a plane wave cutoff of 500 eV for the plane wave expansion of the wave functions was used to obtain highly accurate forces. Because of the magnetic structure of Cr and Fe, spin polarized calculations were considered for all cases. Force tolerance for the structural relaxation was 0.05 eV/Å. Disordered rocksalt was simulated by creating a special quasirandom structure (SQS) [43] with the rocksalt structure, but with the $MgCr_2O_4$ stoichiometry by replacing 3 Mg ions with 2 Cr ions for every structural unit of 4 MgO, as shown in Fig. 4(a) and (b).

Spinel $MgCr_2O_4$ is thermodynamically the most stable phase among all combinations of Mg, Cr and O. However, compared to a disordered rocksalt structure, in which the material has the spinel stoichiometry, but the Mg and Cr cations are randomly distributed in a rocksalt structure, the spinel structure is more stable only by 0.20 eV per atom. Hence, during irradiation the intermixing of Cr into MgO and the formation of disordered rockstalt is possible before the atomic structure of the transition layer settles into the spinel structure (indeed, irradiation causes an order-to-disorder transformation of spinel into rocksalt [44]). Further, the DFT-calculated volume changes, compared to pristine MgO, are −1.9% and −3.1% for disordered-rocksalt-structured and spinel-structured $MgCr_2O_4$, respectively, consistent with the experimental observations that the transition layer has a smaller lattice constant than the MgO substrate. These results suggest that a two-phase transition layer, containing both spinel and disordered rocksalt, is thermodynamically and structurally reasonable.

The transition layer observed contains chromium not iron. This indicates that, upon incorporation into MgO, Cr substitutes for Mg to form either rocksalt or spinel, but Fe does not. To model this process we inserted either one Cr or Fe atom into a 64-atom MgO supercell. The Fe or Cr atom is introduced in either a substitutional or interstitial position (the interstitial position is surrounded by 4 Mg and 4 O atoms [45]). In the substitutional case, the replaced Mg atom was placed in an interstitial position. Structures 1 and 2 in Fig. 4(c) show both the interstitial and substitutional positions, respectively, of Cr or Fe defects within a MgO supercell. Structure 3 in Fig. 4(c) represents Mg farther away from substituted ion as compared to structure 2.

For all structures we calculate the formation energy of both neutral and charged defects. The relative stability of different charge states is compared using the total energy of the system, which is given by

$$E^{Total}(D^q) = E_f^{DFT}(D^q) + qE_F,$$

where $E^{Total}(D^q)$ is the total energy of the system containing a Cr or Fe atom as defect interstitial or substitutional in charge state q and $E_f^{DFT}(D^q)$ is the DFT energy of the charged supercell. More details on the total energy calculations can be found in Janotti et al. [46]. The total energy of the neutral system does not depend on the charge state, while that of a charged supercell depends on the Fermi level E_F of the electron reservoir referenced to the valence-band maximum (VBM) (in this case FeCr). Even for the highest value of E_F, which is the bandgap of MgO (7.8 eV as calculated with DFT), Cr and Fe in MgO are more stable in the 3+ charge state as compared to the neutral state. This type of replacement is consistent with other studies of 3+ aliovalent doping of MgO [47].

In the 3+ charge state, Cr prefers to be in a substitutional as compared to an interstitial position, as indicated in Fig. 4(d). That is, the reaction $Cr_I^{3+} \rightarrow Cr_{Mg}^{1+} + Mg_I^{2+}$ is exothermic; it is favorable for a Cr interstitial to kick-out a Mg ion, forming a substitutional Cr and interstitial Mg. Once Mg is knocked out of its lattice position, it will tend to migrate away from the substitutional Cr due to the electrostatic repulsion between Mg_I^{2+} and Cr_{Mg}^{1+}. Thus, if Cr is knocked into MgO as an interstitial species during the collision cascade events, it will quickly displace sufficient Mg ions from the lattice, forming $MgCr_2O_4$. This is compatible with our HRTEM and EELS observations. On the other hand, the reaction $Fe_I^{3+} \rightarrow Fe_{Mg}^{1+} + Mg_I^{2+}$ is endothermic, see Fig. 4(d). Hence, even if Fe atoms are displaced into MgO and find a preexisting Mg vacancy, any residual Mg interstitials will displace that Fe back into an interstitial position, where they may diffuse back to the metal layer. This difference explains why Cr incorporation into MgO leads to the formation of spinel-like compounds, but the same does not happen when Fe is introduced into MgO.

Together, the experimental and modeling results lead to the following picture for the chemical and structural evolution of the interfacial region under irradiation. By virtue of stronger binding with either oxygen or irradiation-induced point defects compared to Fe, Cr atoms prefer to segregate toward the FeCr/MgO interface under either annealing or irradiation [48–50]. With a layer of enriched Cr initially formed at the interface, the Cr atoms are then introduced randomly, either by radiation-enhanced diffusion or ballistic impact, into the MgO substrate. Fe will also be introduced into MgO via ballistic mixing. However, the Cr will substitute into the MgO structure while Fe will remain as an interstitial species and free to diffuse through the lattice. The inceptive ordering of the resulting Cr–Mg–O phase may be random, consistent with a rocksalt-structured compound. If kinetics allow, the chemistry may order and a spinel compound will eventually precipitate within the transition layer. Further, the propensity for disordering [51–56] depends on the stoichiometry of the spinel, with non-stoichiometric spinels more prone to disorder [52]. Accordingly, in our experiments, depending on the level of Cr substitution, the driving force for ordering into the

spinel structure will be different. Thus, we have competing effects for determining the ultimate structure of the Cr-substituted MgO transition layer. On the one hand, the kinetics associated with irradiation will disrupt the reordering process, driving the system toward the rocksalt structure, while, on the other hand, thermodynamics would drive this chemistry toward spinel. Combining the observations from the experiments and the DFT calculations, we conclude that Cr introduction into MgO leads to a transition layer that contains substitutional Cr ions, which, if the local conditions are conducive, can form $MgCr_2O_4$ spinel.

5. Summary

Fe-12at.Cr thin films were epitaxially grown on a single crystal MgO (100) substrate. The interface exhibited an orientation relationship of MgO (100) ‖ FeCr (100) & MgO [100] ‖ FeCr [110]. Misfit dislocations, with an average spacing of 4.8 nm, were formed at the interface to mitigate the lattice mismatch strain. 10 MeV Ni^{3+} ion irradiation was performed at 500 °C to examine the structural and chemical stability of the interface while concurrent anneals of the as-synthesized material were performed to separate the effects of irradiation. Cr was probed to segregate to the interface thermodynamically. Radiation-induced segregation of Cr from the Fe layer to and across the FeCr/MgO interface was observed. As a result, a two-phase transition layer containing precipitates of a spinel phase along with Cr-rich rocksalt was formed on the MgO side of the FeCr/MgO interface. First-principles calculations show that it is exothermic for interstitial Cr to substitute Mg in MgO, but that Fe prefers to remain as an interstitial. The elemental redistribution and structural reordering we have observed at the FeCr/MgO interface has implications beyond our study. Each of these changes in structure and chemistry can either enhance or degrade material performance and suggest that the properties of pristine materials are not representative of the structures that evolve under irradiation in complex composites. Thus, the interface morphologies in materials such as ODS that are responsible for the interaction with radiation-induced defects may be very different from the as-synthesized interfaces. Finally, this model study suggests irradiation can be used to form new phases and complexions at interfaces that may have new mechanical and functional properties [57,58].

Acknowledgments

We gratefully acknowledge the support of the U.S. Department of Energy through the Los Alamos National Laboratory (LANL)/Laboratory Directed Research & Development (LDRD) Program for this work. This research used resources provided by the LANL Institutional Computing Program. This work was performed, in part, at the Center for Integrated Nanotechnologies, an Office of Science User Facility operated for the U.S. Department of Energy (DOE) Office of Science. LANL, an affirmative action/equal opportunity employer, is operated by Los Alamos National Security, LLC, for the National Nuclear Security Administration of the U.S. Department of Energy under contract DE-AC52-06NA25396. JAA acknowledges access to the ORNL's ShaRE User Facility where part of the TEM work was performed in collaboration with Miaofang Chi and Juan Carlos Idrobo, which are sponsored by the Scientific User Facilities Division, Office of Basic Energy Sciences, U.S. Department of Energy. Y. Xu and H. Luo are affiliates supported by the New Mexico Consortium at LANL.

References

[1] M.W. Finnis, J. Phys.: Condens. Matter 8 (1996) 5811.
[2] F. Ernest, Mater. Sci. Eng. R14 (1995) 97.
[3] M.G. Nicholas, D.A. Mortimer, Mater. Sci. Technol. 1 (1985) 657.
[4] M. Ruhle, A.G. Evans, Mater. Sci. Eng. A 107 (1989) 187.
[5] S.B. Sinnott, E.C. Dickey, Mater. Sci. Eng.: R 43 (2003) 1.
[6] J.M. Howe, Int. Mater. Rev. 38 (1993) 233.
[7] H. Bialas, K. Heneka, Vacuum 45 (1994) 79.
[8] U. Schonberger, O.K. Andersen, M. Methfessel, Acta Metall. Mater. 40 (1992) S1.
[9] P. Lu, F. Cosandey, Ultramicroscopy 40 (1992) 271.
[10] P. Lu, F. Cosandey, Acta Metall. Mater. 40 (1992) S259.
[11] A. Trampert, F. Ernst, C.P. Flynn, H.F. Fischmeister, M. Ruhle, Acta Metall. Mater. 40 (1992) S227.
[12] F.R. Chen, S.K. Chiou, L. Chang, C.S. Hong, Ultramicroscopy 54 (1994) 179.
[13] D.A. Shashkov, M.F. Chisholm, D.N. Seidman, Acta Mater. 47 (1999) 3939.
[14] Y.F. Zhukovskii, E.A. Kotomin, P.W.M. Jacobs, A.M. Stoneham, J.H. Harding, Surf. Sci. 441 (1999) 373.
[15] E. Heifets, Y.F. Zhukovskii, E.A. Kotomin, M. Causa, Chem. Phys. Lett. 283 (1998) 395.
[16] C. Giovanardi, A.d. Bona, T.S. Moia, S. Valeri, C. Pisani, M. Sgroi, M. Busso, Surf. Sci. 505 (2002) L209.
[17] C.-M. Wang, T.C. Kaspar, V. Shutthanandan, A.G. Joly, R.J. Kurtz, Acta Mater. 59 (2011) 4274.
[18] I. Tanaka, M. Mizuno, S. NakaJyo, H. Adachi, Acta Mater. 46 (1998) 6511.
[19] Y. Ikuhara, Y. Sugawara, I. Tanaka, P. Pirouz, Interface Sci. 5 (1997) 5.
[20] Y. Ikuhara, P. Pirouz, S. Yadavalli, C.P. Flynn, Philos. Mag. A 72 (1995) 179.
[21] D.X. Li, P. Pirouz, A.H. Heuer, S. Yadavalli, C.P. Flynn, Acta Metall. Mater. 40 (1992) S237.
[22] E.G. Fu, Y. Fang, M.J. Zhuo, S.J. Zheng, Z.X. Bi, Y.Q. Wang, M. Tang, X. Ding, W.Z. Han, H.M. Luo, J.K. Baldwin, A. Misra, M. Nastasi, Acta Mater. 64 (2014) 100.
[23] G.R. Odette, M.J. Alinger, B.D. Wirth, Annu. Rev. Mater. Res. 38 (2008) 471.
[24] A.G. Certain, K.G. Field, T.R. Allen, M.K. Miller, J. Bentley, J.T. Busby, J. Nucl. Mater. 407 (2010) 2.
[25] T.R. Allen, J. Gan, J.I. Cole, M.K. Miller, J.T. Busby, S. Shutthanandan, S. Thevuthasan, J. Nucl. Mater. 375 (2008) 26.
[26] E.A. Marquis, S. Lozano-Perez, V.d. Castro, J. Nucl. Mater. 417 (2011) 257.
[27] C.A. Williams, J.M. Hyde, G.D.W. Smith, E.A. Marquis, J. Nucl. Mater. 412 (2011) 100.
[28] D. Bhattacharyya, P. Dickerson, G.R. Odette, S.A. Maloy, A. Misra, M.A. Nastasi, Philos. Mag. 92 (2012) 2089.
[29] E.A. Marquis, J.M. Hyde, D.W. Saxey, S. Lozano-Perez, V. de Castro, D. Hudson, C.A. Willaime, S. Humphry-Baker, G.D.W. Smith, Mater. Today 12 (2009) 30.
[30] EA. Marquis, Appl. Phys. Lett. 93 (2008) 181904.
[31] Y. Chen, L. Jiao, C. Sun, M. Song, K.Y. Yu, Y. Liu, M. Kirk, M. Li, H. Wang, X. Zhang, J. Nucl. Mater. 452 (2014) 321.
[32] Y. Xu, J.A. Aguiar, S.K. Yadav, O. Anderoglu, J.K. Baldwin, Y.Q. Wang, J.A. Valdez, A. Misra, H.M. Luo, B.P. Uberuaga, N. Li, Acta Mater. 89 (2015) 364.
[33] R.E. Stoller, M.B. Toloczko, G.S. Was, A.G. Certain, S. Dwaraknath, F.A. Garner, Nucl. Instrum. Meth. Phys. Res. Sect. B 310 (2013) 75.
[34] J.F. Ziegler, M.D. Ziegler, J.P. Biersack, Nucl. Instrum. Meth. Phys. Res. Sect. B 268 (2010) 1818.
[35] <http://www.srim.org>.

[36] H. Sieber, D. Hess, P. Werner, Philos. Mag. A 75 (1997) 889.
[37] C.W. White, C.J. McHargue, P.S. Sklad, L.A. Boatner, G.C. Farlow, Mater. Sci. Rep. 4 (1989) 41.
[38] T. Sonoda, H. Abe, C. Kinoshita, H. Naramoto, Nucl. Instrum. Meth. Phys. Res. Sect. B 127/128 (1997) 176.
[39] L. Jiao, A. Chen, M.T. Myers, M.J. General, L. Shao, X. Zhang, H. Wang, J. Nucl. Mater. 434 (2013) 217.
[40] G. Kresse, J. Furthmuller, Phys. Rev. B 54 (1996) 11169.
[41] J.P. Perdew, K. Burke, M. Ernzerhof, Phys. Rev. Lett. 77 (1996) 3865.
[42] P.E. Blochl, Phys. Rev. B 50 (1994) 17953.
[43] A. Zunger, S.H. Wei, L.G. Ferreira, J.E. Bernard, Phys. Rev. Lett. 65 (1990) 353.
[44] M. Ishimaru, I.V. Afanasyev-Charkin, K.E. Sickafus, Appl. Phys. Lett. 76 (2000) 2556.
[45] T. Brudevoll, E.A. Kotomin, N.E. Christensen, Phys. Rev. B 53 (1996) 7731.
[46] A. Janotti, J.B. Varley, P. Rinke, N. Umezawa, G. Kresse, C.G. Van de Walle, Phys. Rev. B 81 (2010) 085212.
[47] S. Prada, L. Giordano, G. Pacchioni, J. Phys. Chem. C 116 (2012) 5781.
[48] G. Was, B.D. Wirth, Award Number: DE-FC07-07ID14828, 2011.
[49] G.S. Was, J.P. Wharry, B. Frisbie, B.D. Wirth, D. Morgan, J.D. Tucker, T.R. Allen, J. Nucl. Mater. 411 (2011) 41.
[50] J.P. Wharry, Z. Jiao, G.S. Was, J. Nucl. Mater. 425 (2012) 117.
[51] K.E. Sickafus, A.C. Larson, N. Yu, M. Nastasi, G.W. Hollenberg, F.A. Garner, R.C. Bradt, J. Nucl. Mater. 219 (1995) 128.
[52] K.E. Sickafus, N. Yu, M. Nastasi, Nucl. Instrum. Meth. Phys. Res. Sect. B 116 (1996) 85.
[53] C. Kinoshita, S. Matsumura, K. Yasuda, T. Soeda, M. Moujima, Mat. Res. Soc. Symp. Proc. 540 (1999) 287.
[54] K.E. Sickafus, Science 289 (2000) 748.
[55] R. Devanathan, K.E. Sickafus, N. Yu, M. Nastasi, Philos. Mag. Lett. 72 (2006) 155.
[56] N. Yu, K.E. Sickafus, M. Nastasi, Philos. Mag. Lett. 70 (2006) 235.
[57] M.P. Harmer, Science 332 (2011) 182.
[58] F. Lu, M. Lang, M. Huang, F. Namavar, C. Trautmann, R.C. Ewing, J. Lian, Nucl. Instrum. Meth. Phys. Res. Sect. B 286 (2012) 266.